Automatic Extraction of Measurement-Based Large-Signal FET Models by Nonlinear Function Sampling

Teresa M. Martín-Guerrero, *Member, IEEE*, Alberto Santarelli, *Member, IEEE*, Gian Piero Gibiino, *Member, IEEE*, Pier Andrea Traverso, *Member, IEEE*, Carlos Camacho-Peñalosa, *Life Senior Member, IEEE*, and Fabio Filicori

***Abstract*— A new method is proposed for the accurate experimental characterization and fully automated extraction of compact nonlinear models for field-effect transistors (FETs). The approach, which leads to a charge-conservative description, is based on a single large-signal measurement under a two-tone sinusoidal wave excitation. A suitable choice of tone frequencies, amplitudes, and bias allows to adequately characterize the transistor over the whole safe operating region. The voltage-controlled nonlinear functions describing the two-port FET model can be computed over an arbitrarily dense voltage domain by solving an overdetermined system of linear equations. These equations are expressed in terms of a new nonlinear function sampling operator based on a biperiodic Fourier series description of the acquired frequency spectra. The experimental validation is carried out on a 0.25-μm gallium nitride (GaN) on silicon carbide (SiC) high-electron-mobility transistor (HEMT) under continuous-wave (CW) and two-tone excitation (intermodulation distortion test).**

***Index Terms*— Field-effect transistors (FETs), gallium nitride (GaN), large-signal measurements, nonlinear vector network analyzer (NVNA), semiconductor device modeling.**

I. Introduction

THE extraction of compact nonlinear field-effect transistor (FET) models for microwave applications often relies on multibias S-parameter measurements [1], [2]. However, these identification methods are typically affected by several problems, e.g., they usually allow only for a partial exploration of the voltage domain due to self-heating. In addition, path-dependent integration of differential parameters is frequently observed, due to temperature and charge trapping variations across the bias conditions [3].

Manuscript received July 31, 2019; revised December 26, 2019; accepted December 30, 2019. Date of publication March 27, 2020; date of current version May 5, 2020. This work was supported in part by the Spanish Ministerio de Ciencia, Innovación y Universidades in the frame of Salvador de Madariaga Program under Grant PRX18/00108. *(Corresponding author: Teresa M. Martín-Guerrero.)*

Teresa M. Martín-Guerrero and Carlos Camacho-Peñalosa are with the Departamento de Ingeniería de Comunicaciones, Universidad de Málaga, 29010 Málaga, Spain (e-mail: teresa@ic.uma.es).

Alberto Santarelli, Gian Piero Gibiino, Pier Andrea Traverso, and Fabio Filicori are with the Department of Electrical, Electronic, and Information Engineering (DEI) Guglielmo Marconi, University of Bologna, 40136 Bologna, Italy (e-mail: alberto.santarelli@unibo.it).

Color versions of one or more of the figures in this article are available online at http://ieeexplore.ieee.org.

Digital Object Identifier 10.1109/TMTT.2020.2968886

The adoption of narrow pulse current [4]–[9] and S-parameter measurement techniques [4], [6], [7] allows for isothermal and isotrap state (i.e., isodynamic) FET characterization. Nevertheless, these pulsed techniques make use of model identification experiments under very specific operating conditions, which are quite different from the continuous-wave (CW)-like regimes of large-signal power amplifier (PA) applications. Generalizing the models to account for those different operating regimes in the presence of charge trapping can become a complex task, especially considering particular cases such as the trap-induced nonlinear dynamic behavior displayed by gallium nitride (GaN) HEMTs [8]. In this context, model extraction procedures based on large-signal CW or modulated excitations represent an attractive possibility [10]–[23]. Some of these approaches exploit artificial neural networks [11], which feature powerful fitting capabilities to obtain the conduction current and the charge functions from a large amount of data under different bias, radio frequency (RF) excitation, and impedance terminations. Other methods are aimed at a preliminary separation between the conduction and displacement of current components [12]–[23]. In [12] and [13], this separation was obtained by exploiting the constraints between the real and imaginary parts of complex Fourier coefficients of measured waveforms for a single-port device. A simulation-based extension of this approach to the two-port case was proposed in [14]. In [23], a characterization method relying on a two-tone, two-port excitation was used for model extraction. The separation of conduction and displacement currents exploited a point-by-point local approximation of the large-signal regime. Isodynamic voltage-dependent small-signal conductance and capacitance functions were integrated into the frequency domain to obtain quasi-static model functions.

In this article, a new approach for the extraction of conduction I/V and quasi-static charge Q/V functions from large-signal measurements is proposed. The method relies on quasi-periodic two-tone, two-port sinusoidal excitation of transistors as in the experiment described in [23] and on constraints between the real and imaginary parts of Fourier coefficients of waveforms analogous to [14]. This formulation allows for the direct extraction of conduction current and charge waveforms' spectral coefficients. A new nonlinear function sampling (NFS) operator is introduced and used

for generating arbitrarily dense model functions. The extraction procedure is formulated to display linear dependence on the unknown quantities, leading to an automatic, robust, and unambiguous identification that avoids the use of nonlinear optimization or integration procedures. The resulting model functions can be described as simple lookup tables (LUTs) or can be easily replaced by analytical approximating functions according to the user preference.

This article is structured as follows. The measurement procedure and the differences between the quasi-periodic experiment and the actual periodic approximation are addressed in Section II. Section III deals with the introduction of the NFS operator. This operator is exploited in Section IV, where the model extraction method is proposed. The application of the procedure for a 0.25-μm GaN-on-silicon-carbide (SiC) HEMT and its experimental validation is discussed in Section V. Conclusions are finally drawn in Section VI.

II. Two-Tone, Two-Port Device Modeling

A. Characterization Under Quasi-Periodic Regime

Let us consider a specific experimental procedure in which the device under test (DUT), i.e., an FET in common-source configuration, is excited at the two gate and drain ports by two single-tone power waves at independent and incommensurable frequencies f_A and f_B [23]. One tone is applied at each port. The absolute (power and phase) incident and reflected waves are measured at the extrinsic transistor ports; extrinsic voltages and currents are then obtained through well-known linear transformations. Given the device nonlinearity, mixing products are generated in both voltages and currents at frequencies $f_{n,m} = |nf_A + mf_B|$, with $n, m = 0, \pm1, \pm2, \ldots$ ($r = |n| + |m|$ is the mixing order).

After deembedding of the extrinsic parasitic network, one obtains the intrinsic spectral components (complex quantities) of transistor voltages $\underline{V}_{n,m} = \{V_{Gn,m}, V_{Dn,m}\}^T$ and currents $\underline{I}_{n,m} = \{I_{Gn,m}, I_{Dn,m}\}^T$, where symbol $\{\cdot\}^T$ stands for vector transposition. The corresponding time-domain waveforms are linked to their spectra by the Fourier analysis

$$\underline{\mathcal{I}}(t) = \mathrm{Re}\left\{\sum_{n,m} \underline{I}_{n,m}\, e^{j(n\omega_A + m\omega_B)t}\right\} \tag{1}$$

$$\underline{\mathcal{V}}(t) = \mathrm{Re}\left\{\sum_{n,m} \underline{V}_{n,m}\, e^{j(n\omega_A + m\omega_B)t}\right\} \tag{2}$$

where the coefficients have been ordered in terms of the two excitation frequencies, with $\underline{\mathcal{I}} = \{\mathcal{I}_G, \mathcal{I}_D\}^T$, $\underline{\mathcal{V}} = \{\mathcal{V}_G, \mathcal{V}_D\}^T$, $\omega_A = 2\pi f_A$, and $\omega_B = 2\pi f_B$.

In order to ensure well-conditioned waveform acquisitions for FET modeling, first, f_A and f_B must be sufficiently high to stimulate not only the conduction current but also substantial displacement current components; second, the mixing products must fall in a portion of the frequency spectra where no spurious memory effects are excited. In practice, the spectral lines should lie above the cutoff of the low-frequency dispersive phenomena due to charge trapping and self-heating. At the same time, they must not extend to very high frequencies, in order to avoid nonquasi-static effects associated with junction charge storage.

Due to the beat between the two incommensurable frequencies, the instantaneous gate and drain voltages densely swing across a certain portion of the operative domain $\mathcal{D}_v$, where this portion is set by the chosen tone amplitudes [2]. In effect, given a sufficiently long observation time, any point inside the outer bound of $\mathcal{D}_v$ would be reached. In the frequency domain, no multiple products will land on the same frequency bin, thus obtaining the separation among all the mixing products. In other words, each spectral line will correspond to a single intermodulation product, and the minimum frequency spacing between the products would tend to be infinitesimal if unlimited mixing orders were considered. As the transistor dynamically experiences an extremely wide set of equivalent source and load terminations [18], a great amount of information can be extracted from this kind of regime for modeling purposes.

From a practical point of view, a finite observation time must be adopted for acquiring the incident and reflected waves, resulting in a discrete frequency grid defined by a minimum frequency, and by a minimum frequency step. It should be noted that the available instrumentation used for accurate large-signal network analysis is based on coherent receivers, which must be frequency-locked with the synthesizers. In addition, commercial mixer-based architectures for large-signal network analysis at microwaves rely on a phase reference usually provided by a comb generator device, which produces an harmonic frequency grid. Also, a suitable truncation of spectra to finite maximum harmonic orders, $|n| \leq N$, $|m| \leq M$, and $r \leq R$, should inevitably be considered. Thus, an excitation with two tones at commensurable frequencies is eventually chosen, leading to a periodic regime with fundamental frequency f_F given by the greatest common divisor of the two numbers f_A and f_B, i.e., $f_F = \mathrm{GCD}(f_A f_B)$. In this case, the instantaneous voltage path traveled over the voltage plane during the period ($T_F = 1/f_F$) only touches a well-determined locus of points within the transistor operating range. Thus, a poor choice of frequency values could lead to inadequate voltage loci for the extraction of I/V and Q/V characteristics over the whole transistor safe operating area. However, transistor operation akin to the quasi-periodic case is substantially obtained by choosing two frequencies that guarantee nonoverlapping mixing products up to a certain order.

In this article, a setup based on a mixer-based nonlinear vector network analyzer (NVNA) has been used for the experiment (see Fig. 1), featuring a 10-MHz harmonic phase reference up to 67 GHz. Thus, $f_A = 2$ GHz and $f_B = 2.74$ GHz were chosen, resulting in $f_F = 20$ MHz. Considering that the DUT is a 0.25-μm GaN-on-SiC HEMT, the GHz range is suitable for both frequencies, with a spacing shorter than an octave, i.e., $1 < f_B/f_A < 2$. The spectra were measured by assuming $N = 10$, $M = 10$, and $R = 20$, leading to $N_B = 220$ frequency bins. The minimum mixing product is obtained at $f_{\min} = 220$ MHz, and the minimum frequency spacing is $\Delta f_{\min} = 4f_F = 80$ MHz. The maximum frequency in the measured spectra is $f_{\max} = 47.4$ GHz.

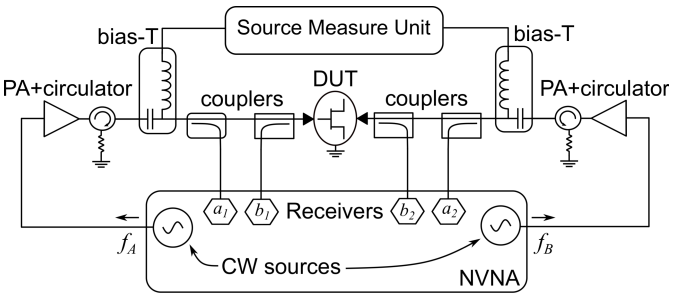

(a)

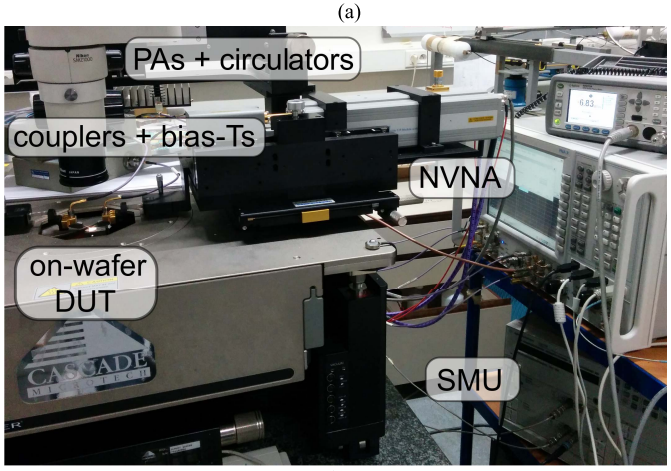

(b)

Fig. 1. (a) Block diagram and (b) photograph of the measurement setup.

B. Bitemporal Waveform Analysis

When adopting a quasi-periodic excitation (or equivalently, its periodic approximation), a signal description based on multidimensional Fourier series [24] can be effectively used in order to extract information from the waveforms spanning the whole voltage plane. This technique is based on the introduction of an auxiliary bitemporal domain (τ_A, τ_B) in such a way that the quasi-periodic signals can be more efficiently treated as biperiodic ones. According to this technique, the expressions in (1) and (2) are replaced by

$$\underline{\mathcal{I}}(\tau_A, \tau_B) \doteq \mathrm{Re}\left\{\sum_{n,m} \underline{I}_{n,m}\, e^{j(n\omega_A\tau_A + m\omega_B\tau_B)}\right\} \tag{3}$$

$$\underline{\mathcal{V}}(\tau_A, \tau_B) \doteq \mathrm{Re}\left\{\sum_{n,m} \underline{V}_{n,m}\, e^{j(n\omega_A\tau_A + m\omega_B\tau_B)}\right\}. \tag{4}$$

Cleary, the bitemporal functions defined by (3) and (4) coincide with the ones in (1) and (2) only for $\tau_A = \tau_B = t$. On the other hand, both (3) and (4) have the advantage of being periodic along the two auxiliary time axes τ_A and τ_B, with periods $T_A = 2\pi/\omega_A$ and $T_B = 2\pi/\omega_B$, respectively. Due to the continuity of the sinusoidal waveforms in (3) and (4) with respect to τ_A and τ_B, any voltage pair (v_G, v_D) in the voltage domain $\mathcal{D}_v$ can be obtained with a suitable choice of the (τ_A, τ_B) auxiliary time variables. In other words, any voltage pair (v_G, v_D) can be reached, provided that a sufficiently dense discretization is adopted along the two periodic auxiliary axes τ_A and τ_B.

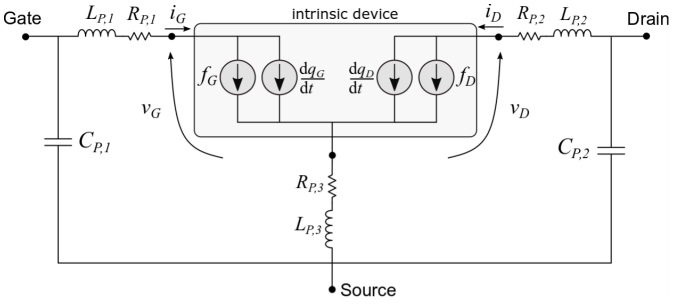

Fig. 2. FET equivalent circuit including parasitic elements. The conduction drain current f_D represents a specific isodynamic condition. To account for thermal and trapping effects, f_D is substituted by f'_D as in Section V.

In the following Fourier series expansions, we will separate real and imaginary parts of spectral components. For instance, by considering the unilateral current spectral components $\underline{I}_{n,m}$, we let

$$\underline{I}_{n,m} = \underline{I}^a_{n,m} - j\underline{I}^b_{n,m} \tag{5}$$

where $\underline{I}^a_{n,m}$ and $\underline{I}^b_{n,m}$ are now vectors of real quantities. Thus, (3) becomes

$$\underline{\mathcal{I}}(\tau_A, \tau_B) \doteq \underline{I}_{0,0} + \sum_{n,m} \underline{I}^a_{n,m} \cos(n\omega_A\tau_A + m\omega_B\tau_B) + \sum_{n,m} \underline{I}^b_{n,m} \sin(n\omega_A\tau_A + m\omega_B\tau_B). \tag{6}$$

The spectral coefficients $\underline{V}^a_{n,m}$ and $\underline{V}^b_{n,m}$ are defined accordingly.

C. Intrinsic Quasi-Static FET Model Formulation

According to the particular characterization adopted in this article, a quasi-static intrinsic transistor model (see Fig. 2) can be assumed, that is

$$\underline{i}(\underline{v}) = \underline{f}(\underline{v}) + \frac{d\underline{q}(\underline{v})}{dt} \tag{7}$$

with $\underline{i} = \{i_G, i_D\}^T$ and $\underline{v} = \{v_G, v_D\}^T$. The $\underline{f}(\underline{v}) = \{f_G(\underline{v}), f_D(\underline{v})\}^T$ functions in (7) represent isodynamic I/V input and output FET conduction characteristics. The vector $\underline{q}(\underline{v}) = \{q_G(\underline{v}), q_D(\underline{v})\}^T$ includes the gate and drain quasi-static charge functions. It is to be noted that, in general, the thermal and trapping state associated with the particular operating regime depends on the bias condition and on the excitation signals. Thus, different excitation conditions generally involve different extracted $\underline{f}(\underline{v})$ and $\underline{q}(\underline{v})$ (see Section V).

The extraction method here proposed leads to a direct identification of the conduction characteristics $\underline{f}(\underline{v})$ and the displacement charge functions $\underline{q}(\underline{v})$ on the basis of the measured voltage and current spectral components $\underline{V}_{n,m}$, $\underline{I}_{n,m}$ at the intrinsic plane. After deembedding the parasitic network, the method is almost automatic. In fact, it is based on the solution of linear systems (thus avoiding convergence problems of nonlinear optimization algorithms) and it does not require any choice by the operator, apart from the definition of reasonable time- and voltage-domain discretization grids (see Section V).

For an assigned set of voltage waveforms $\underline{\mathcal{V}}(t) \equiv \underline{v}(t)$, the quasi-static current $\underline{\mathcal{I}}(t)$ predicted by model (7) is given by

$$\underline{\mathcal{I}}(t) = \underline{\mathcal{F}}(t) + \frac{d\underline{\mathcal{Q}}(t)}{dt} \tag{8}$$

where $\underline{\mathcal{F}}(t)$ and $\underline{\mathcal{Q}}(t)$ are two set of (yet unknown) waveforms describing the conduction transistor response and the evolution of the charge function values over time. Coherently, in the bitemporal domain, $\underline{\mathcal{F}}$ and $\underline{\mathcal{Q}}$ can be defined as

$$\underline{\mathcal{I}}(\tau_A,\, \tau_B) \doteq \underline{\mathcal{F}}(\tau_A,\, \tau_B) + \frac{\partial \underline{\mathcal{Q}}(\tau_A,\, \tau_B)}{\partial \tau_A} + \frac{\partial \underline{\mathcal{Q}}(\tau_A,\, \tau_B)}{\partial \tau_B}. \tag{9}$$

Clearly, it holds

$$\underline{\mathcal{I}}(\tau_A,\, \tau_B) = \underline{i}\left(\underline{\mathcal{V}}(\tau_A,\, \tau_B)\right) \tag{10}$$

$$\underline{\mathcal{F}}(\tau_A,\, \tau_B) = \underline{f}\left(\underline{\mathcal{V}}(\tau_A,\, \tau_B)\right) \tag{11}$$

$$\underline{\mathcal{Q}}(\tau_A,\, \tau_B) = \underline{q}\left(\underline{\mathcal{V}}(\tau_A,\, \tau_B)\right) \tag{12}$$

where $\underline{\mathcal{V}}(\tau_A,\, \tau_B)$ are the bitemporal voltage waveforms. Spectral components $\underline{F}^a_{n,m}$ and $\underline{F}^b_{n,m}$ associated with $\underline{\mathcal{F}}(\tau_A,\, \tau_B)$ and $\underline{Q}^a_{n,m}$ and $\underline{Q}^b_{n,m}$ associated with $\underline{\mathcal{Q}}(\tau_A,\, \tau_B)$ lead to

$$\begin{aligned}\underline{\mathcal{F}}(\tau_A,\, \tau_B) \doteq\ & \underline{F}_{0,0} + \sum_{n,m} \underline{F}^a_{n,m} \cos\left(n\omega_A\tau_A + m\omega_B\tau_B\right) \\ & + \sum_{n,m} \underline{F}^b_{n,m} \sin\left(n\omega_A\tau_A + m\omega_B\tau_B\right)\end{aligned} \tag{13}$$

$$\begin{aligned}\underline{\mathcal{Q}}(\tau_A,\, \tau_B) \doteq\ & \sum_{n,m} \underline{Q}^a_{n,m} \cos\left(n\omega_A\tau_A + m\omega_B\tau_B\right) \\ & + \sum_{n,m} \underline{Q}^b_{n,m} \sin\left(n\omega_A\tau_A + m\omega_B\tau_B\right)\end{aligned} \tag{14}$$

where $\underline{I}_{0,0} = \underline{F}_{0,0}$ as in (9). In addition, since $\underline{Q}_{0,0}$ is an irrelevant and unknown quantity, it will be arbitrarily chosen equal to zero. The derivative of (14) with respect to the two auxiliary time variables $(\tau_A,\, \tau_B)$ leads to

$$\begin{aligned}&\frac{\partial \underline{\mathcal{Q}}(\tau_A,\, \tau_B)}{\partial \tau_A} + \frac{\partial \underline{\mathcal{Q}}(\tau_A,\, \tau_B)}{\partial \tau_B} \\ &\quad = \sum_{n,m} \left(n\omega_A + m\omega_B\right)\, \underline{Q}^b_{n,m} \cos\left(n\omega_A\tau_A + m\omega_B\tau_B\right) \\ &\qquad - \sum_{n,m} \left(n\omega_A + m\omega_B\right)\, \underline{Q}^a_{n,m} \sin\left(n\omega_A\tau_A + m\omega_B\tau_B\right).\end{aligned} \tag{15}$$

Thus, on the basis of (6), (13), and (15), the quasi-static current model (9) can be written in terms of the following spectral balance equations, for each n and m:

$$\begin{aligned}\underline{I}^a_{n,m} &= \underline{F}^a_{n,m} + \omega_{nm}\, \underline{Q}^b_{n,m} \\ \underline{I}^b_{n,m} &= \underline{F}^b_{n,m} - \omega_{nm}\, \underline{Q}^a_{n,m}\end{aligned} \tag{16}$$

where $\omega_{n,m} = 2\pi f_{n,m} = 2\pi\,|nf_A + mf_B|$.

III. Nonlinear Function Sampling

The quasi-static model in spectral balance form (16) represents the basis for the identification of conduction current and charge waveform spectral coefficients. Additional constraints, which are needed for a well-conditioned extraction, will be derived in Section IV by imposing that conduction current

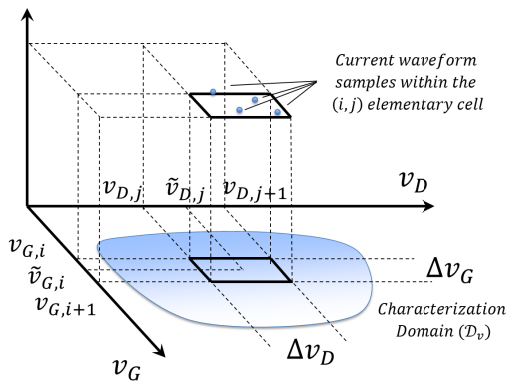

Fig. 3. Elementary cell $(i,\, j)$ over the gate and drain voltage domain $\mathcal{D}_v$.

$\underline{f}(\underline{v})$ and quasi-static charge $\underline{q}(\underline{v})$ characteristics must be memoryless (i.e., algebraic) functions of voltages, according to quasi-static model assumptions.

To this aim, an NFS operator, linking algebraic voltage functions and corresponding time-domain waveforms, is introduced in this section. This operator will both simplify the formulation of the spectral coefficients identifying equations and allow for a straightforward evaluation of the conduction current and charge functions over an arbitrarily dense voltage grid based on their bitemporal waveforms.

Let $v_{G\min}$, $v_{G\max}$, $v_{D\min}$, and $v_{D\max}$ be the extremes of the gate and drain voltage domain $\mathcal{D}_v$ corresponding to a particular set of FET excitation waves. The gate/drain voltage plane is partitioned into a set of elementary cells defined by an $N_G \times N_D$ discretization grid. Grid node voltages $\underline{v}_{i,j} = \{v_{Gi}\, v_{Dj}\}^T$ with $i = 0,\, 1,\, \ldots,\, N_G - 1$ and $j = 0,\, 1,\, \ldots,\, N_D - 1$ define elementary cells with dimensions $\Delta v_G = \left(v_{G\max} - v_{G\min}\right)/N_G$ and $\Delta v_D = \left(v_{D\max} - v_{D\min}\right)/N_D$. Pairs of indexes $(i,\, j)$ identify one cell and its central point $\underline{\tilde{v}}_{i,j} = \{\tilde{v}_{Gi},\, \tilde{v}_{Dj}\}^T$, as shown in Fig. 3.

Let us now consider a generic algebraic voltage function $\varphi(\underline{v})$, whose corresponding time-domain waveform is given by $\phi(\tau_A, \tau_B) = \varphi(\underline{\mathcal{V}}(\tau_A, \tau_B))$ in the presence of an assigned biperiodic $(T_A,\, T_B)$ excitation with intrinsic voltage waveforms $\underline{\mathcal{V}}(\tau_A, \tau_B)$. Any generic voltage $\underline{v} = \{v_G\,, v_D\}^T$ within the characterization domain $\mathcal{D}_v$ belongs to a certain elementary voltage cell $(i,\, j)$ with

$$i = \operatorname{int}\left\{\frac{v_G - v_{G\min}}{\Delta v_G}\right\}, \quad j = \operatorname{int}\left\{\frac{v_D - v_{D\min}}{\Delta v_D}\right\} \tag{17}$$

where $\operatorname{int}\{\cdot\}$ extracts the integer part. Under the operation considered, we introduce here the NFS operator, linking the waveform $\phi\,(\tau_A, \tau_B)$ to its parent nonlinear function $\varphi\,(\underline{v})$

$$\begin{aligned}\varphi(\underline{v}) &= \mathrm{NFS}\{\phi, \underline{v}\} \\ &= \lim_{\Delta\underline{v}\to\underline{0}} \frac{\iint_{T_A,T_B} \phi(\tau_A, \tau_B)\, \Delta\left(\underline{\mathcal{V}}(\tau_A, \tau_B) - \underline{\tilde{v}}_{i,j},\, \Delta\underline{v}\right) d\tau_A\, d\tau_B}{\iint_{T_A,T_B} \Delta\left(\underline{\mathcal{V}}(\tau_A, \tau_B) - \underline{\tilde{v}}_{i,j},\, \Delta\underline{v}\right) d\tau_A\, d\tau_B}\end{aligned} \tag{18}$$

where $\Delta\underline{v} = \{\Delta v_G,\ \Delta v_D\}^T$ and

$$\Delta(\underline{v},\ \Delta\underline{v}) = \begin{cases} 1, & -\dfrac{\Delta v_G}{2} \le v_G < \dfrac{\Delta v_G}{2};\ -\dfrac{\Delta v_D}{2} \le v_D < \dfrac{\Delta v_D}{2} \\ 0, & \text{elsewhere.} \end{cases} \quad (19)$$

Once the waveform is known, the operator allows the computation of the corresponding voltage function all over the characterization domain. The value of the function φ over a generic elementary voltage cell is obtained as the average of the waveform ϕ values falling within the cell. Clearly, the elementary cell dimensions Δv_G and Δv_D must be chosen small enough to guarantee an adequate approximation of the φ function. In fact, according to (18), the NFS operator defines a continuous function with $v_G = \tilde{v}_{G,i}$ and $v_D = \tilde{v}_{D,j}$ as those incremental dimensions approach zero. In practice, finite Δv_G and Δv_D steps will lead to a piecewise approximation of the function. Obviously, the auxiliary time axes τ_A and τ_B must also be discretized. Let us assume L time instants $\tau_{A,l} = l\,\Delta\tau_A$ with $l = 0,\ 1,\ \ldots,\ L-1 (\Delta\tau_A = T_A/L)$ and K time instants $\tau_{B,k} = k\,\Delta\tau_B$ with $k = 0,\ 1,\ \ldots,\ K-1 (\Delta\tau_B = T_B/K)$. In this case, the NFS operator is replaced by

$$\varphi\left(\underline{v}\right) = \mathrm{NFS}\left\{\phi, \underline{v}\right\} = \lim_{\Delta\underline{v}\to\underline{0}} \frac{\sum_{l,k=0}^{L-1,K-1} \phi(\tau_{A,l}, \tau_{B,k})\,\Delta(\underline{\mathcal{V}}_{l,k} - \underline{\tilde{v}}_{i,j},\ \Delta\underline{v})}{\sum_{l,k=0}^{L-1,K-1} \Delta(\underline{\mathcal{V}}_{l,k} - \underline{\tilde{v}}_{i,j},\ \Delta\underline{v})} \quad (20)$$

where it is assumed: $\underline{\mathcal{V}}_{l,k} = \underline{\mathcal{V}}\left(\tau_{A,l}, \tau_{B,k}\right)$. It is worth noting that, by reducing the discretization steps $\Delta\underline{\tau} = \{\Delta\tau_A\ ,\ \Delta\tau_B\}^T$, any number of samples can be obtained within any elementary cell due to the bitemporal interpolation. For instance, if $\underline{s} = \left|d\underline{\mathcal{V}}/dt\right|_{\max}$ were the vector of maximum slopes of the voltage waveforms, at least two points in each elementary cell would be obtained by choosing $\Delta\underline{\tau} < \Delta\underline{v}/2\underline{s}$. In practice, since the model extraction is based on a global system of linear equations in the unknown spectral waveform components, a reasonable number of time samples (not necessarily involving samples in any voltage elementary cell) can be easily obtained, as will be demonstrated in Section IV.

IV. FET Model Extraction Procedure

Transistor model extraction on the basis of the known intrinsic current spectral components $\underline{I}^a_{n,m}$ and $\underline{I}^b_{n,m}$ is done in two main steps: 1) identification of the whole set of complex coefficients $\underline{F}^a_{n,m}$, $\underline{F}^b_{n,m}$, $\underline{Q}^a_{n,m}$, and $\underline{Q}^b_{n,m}$ entirely defining the conduction current and displacement charge waveforms and 2) extraction of the conduction I/V transistor characteristics $\underline{f}\left(\underline{v}\right)$ and Q/V charge functions $\underline{q}\left(\underline{v}\right)$ from their parent waveforms.

The empirical waveforms of intrinsic currents $\underline{\mathcal{I}}(\tau_A,\ \tau_B)$ at the transistor intrinsic ports have been related through (9) to the corresponding waveforms of purely conduction currents $\underline{\mathcal{F}}(\tau_A,\ \tau_B)$ and displacement charges $\underline{\mathcal{Q}}(\tau_A,\ \tau_B)$. These waveforms are associated with algebraic characteristics $\underline{f}\left(\underline{v}\right)$ and $\underline{q}\left(\underline{v}\right)$ appearing in the quasi-static model (7), yet to be extracted. According to the definition of the NFS operator (20), we have

$$\underline{f}(\underline{v}) = \mathrm{NFS}\{\underline{\mathcal{F}}, \underline{v}\} \quad (21)$$

$$\underline{q}(\underline{v}) = \mathrm{NFS}\{\underline{\mathcal{Q}}, \underline{v}\}. \quad (22)$$

With the time discretization $\Delta\tau_A$ and $\Delta\tau_B$ adopted, let $P_{i,j}$ be the number of samples falling into the $(i,\ j)$ elementary voltage cell. In addition, let $\{\underline{\mathcal{V}}(\tau_{A,lp}, \tau_{B,kp})\}_{i,j}$, with $p = 0,\ 1, \ldots,\ P_{i,j} - 1$, be the intrinsic voltage samples falling into the $(i,\ j)$ cell. Only the cells with $P_{i,j} \ge 2$ will contribute to model extraction.

Since the $\underline{\mathcal{F}}$ and $\underline{\mathcal{Q}}$ waveforms derive from algebraic voltage functions $\underline{f}\left(\underline{v}\right)$ and $\underline{q}\left(\underline{v}\right)$, then each pth sample within any $(i,\ j)$ voltage cell must satisfy

$$\underline{\mathcal{F}}(\tau_{A,l_p}\tau_{B,k_p}) = \underline{f}(\underline{\tilde{v}}_{i,j}) \quad (23)$$

$$\underline{\mathcal{Q}}(\tau_{A,l_p}\tau_{B,k_p}) = \underline{q}(\underline{\tilde{v}}_{i,j}) \quad (24)$$

where the second-term quantities may be evaluated by (21) and (22) as

$$\underline{f}(\underline{\tilde{v}}_{i,j}) = \mathrm{NFS}\{\underline{\mathcal{F}}, \underline{\tilde{v}}_{i,j}\} \simeq \frac{1}{P_{i,j}} \sum_{p=0}^{P_{i,j}-1} \underline{\mathcal{F}}(\tau_{A,l_p}, \tau_{B,k_p}) \quad (25)$$

$$\underline{q}(\underline{\tilde{v}}_{i,j}) = \mathrm{NFS}\{\underline{\mathcal{Q}}, \underline{\tilde{v}}_{i,j}\} \simeq \frac{1}{P_{i,j}} \sum_{p=0}^{P_{i,j}-1} \underline{\mathcal{Q}}(\tau_{A,l_p}, \tau_{B,k_p}). \quad (26)$$

Thus, by replacing (25) and (26) into (23) and (24), we finally obtain

$$\underline{\mathcal{F}}(\tau_{A,l_p}, \tau_{B,k_p}) \simeq \frac{1}{P_{i,j}} \sum_{p=0}^{P_{i,j}-1} \underline{\mathcal{F}}(\tau_{A,l_p}, \tau_{B,k_p}) \quad (27)$$

$$\underline{\mathcal{Q}}(\tau_{A,l_p}, \tau_{B,k_p}) \simeq \frac{1}{P_{i,j}} \sum_{p=0}^{P_{i,j}-1} \underline{\mathcal{Q}}(\tau_{A,l_p}, \tau_{B,k_p}). \quad (28)$$

These constraints can be set for each $(\tau_{A,l_p}, \tau_{B,k_p})$ sample held into each $(i,\ j)$ elementary voltage cell, for a total of $P = \sum_{i,j(P_{i,j}\ge 2)} P_{i,j}$ times. For the sake of notation compactness, let us assume

$$\{\theta_{n,m,l_p,k_p}\}_{i,j} = n\omega_A\tau_{A,l_p} + m\omega_B\tau_{B,k_p} \quad (29)$$

where the ij indexes indicate that p may assume values $0, \ldots, P_{i,j} - 1$. In addition, we assume

$$\langle \mathrm{f_T}\{\theta_{n,m,l_p,k_p}\}_{i,j} \rangle_p = \frac{1}{P_{i,j}} \sum_{p=0}^{P_{i,j}-1} \mathrm{f_T}\{\theta_{n,m,l_p,k_p}\}_{i,j} \quad (30)$$

where $\mathrm{f_T}$ is either the $\cos\{\cdot\}$ or $\sin\{\cdot\}$ trigonometric function. With analogous notation, let it finally be

$$\Delta\mathrm{f_T}\{\theta_{n,m,l_p,k_p}\}_{i,j} = \mathrm{f_T}\{\theta_{n,m,l_p,k_p}\}_{i,j} - \langle \mathrm{f_T}\{\theta_{n,m,l_p,k_p}\}_{i,j} \rangle_p. \quad (31)$$

Then, (27) and (28) can be easily transformed by using the Fourier series (13) and (14) into

$$\sum_{n,m} \underline{F}^{a}_{n,m} \Delta\cos\{\theta_{n,m,l_p,k_p}\}_{i,j} + \sum_{n,m} \underline{F}^{b}_{n,m} \Delta\sin\{\theta_{n,m,l_p,k_p}\}_{i,j} \simeq 0 \tag{32}$$

$$\sum_{n,m} \underline{Q}^{a}_{n,m} \Delta\cos\{\theta_{n,m,l_p,k_p}\}_{i,j} + \sum_{n,m} \underline{Q}^{b}_{n,m} \Delta\sin\{\theta_{n,m,l_p,k_p}\}_{i,j} \simeq 0. \tag{33}$$

Due to the spectral balance form in (16), (32) can also be expressed in terms of the charge spectral components. In particular, after simple algebraic manipulation, it holds

$$\sum_{n,m} \omega_{n,m}\, \underline{Q}^{b}_{n,m}\, \Delta cos\{\theta_{n,m,l_p,k_p}\}_{i,j} + \sum_{n,m} \omega_{n,m}\, \underline{Q}^{a}_{n,m} \Delta\sin\{\theta_{n,m,l_p,k_p}\}_{i,j} \simeq \sum_{n,m} \left(\underline{I}^{a}_{n,m} \Delta\cos\{\theta_{n,m,l_p,k_p}\}_{i,j} + \underline{I}^{b}_{n,m} \Delta\sin\{\theta_{n,m,l_p,k_p}\}_{i,j}\right). \tag{34}$$

Finally, by imposing the constraints (33) and (34) for each set of $P_{i,j}$ bitemporal samples within each $(i,\ j)$ voltage cell (only cells with $P_{i,j} \geq 2$ included), an overdetermined linear system of equations is obtained to be solved with respect to the set of $4N_B$ unknown spectral components $\underline{Q}^{a}_{n,m}$ and $\underline{Q}^{b}_{n,m}$ of the complex displacement charge (gate and drain). Once the system is solved, the conduction spectral components, $\underline{F}^{a}_{n,m}$ and $\underline{F}^{b}_{n,m}$, are also obtained by (16).

As a general rule, proper equation weighting is mandatory for a well-conditioned system solution. In this article, each voltage cell was weighted equally over the voltage plane, independently of the number of time samples falling into each cell. Therefore, a weight inversely proportional to $P_{i,j}$ was associated with each equation for each p value with $\underline{\mathcal{V}}(\tau_{A,lp}, \tau_{B,kp})$ within the $(i,\ j)$ cell. In addition, since all the system equations should be dimensionally coherent, the charge constraints (33) were weighted proportionally to the constant angular frequency $\omega_0 = (\omega_A + \omega_B)/2$.

Once the waveforms $\underline{\mathcal{F}}(\tau_A,\ \tau_B)$ and $\underline{\mathcal{Q}}(\tau_A,\ \tau_B)$ have been extracted, the isodynamic gate and drain I/V characteristics $\underline{f}(\underline{v})$ and Q/V charge functions $\underline{q}(\underline{v})$ can be obtained (see Section V). To this aim, direct application of the NFS operator leads to the final goal according to (21) and (22). Any arbitrarily dense grid of voltages can be generated, possibly the same used for solving the linear system of (33) and (34), provided that an adequate discretization is assumed for the bitemporal domain. In this article, the obtained functions have been stored into LUTs but may also be approximated through analytical functions [25], [26].

V. Experimental Results

The modeling procedure described in Section IV was applied to a 8×125 μm (1-mm) GaN-on-SiC HEMT in 0.25-μm technology. The DUT was biased at $I_{DQ} \simeq 80$ mA and $V_{DQ} = 30$ V. As discussed in Section II-A, $f_A = 2$ GHz and $f_B = 2.74$ GHz were chosen for the two-tone two-port characterization. The synthesizers available input powers were $P_A = 18$ dBm and $P_B = 36$ dBm at the gate and drain ports, respectively. NVNA measurements were performed by means of a Keysight PNA-X N5247A (see Fig. 1).

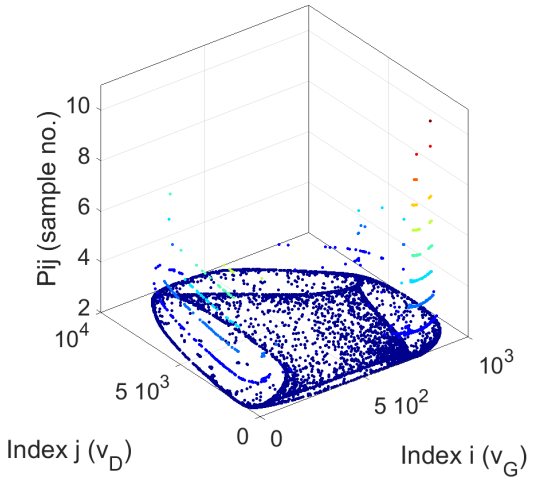

Fig. 4. Number of samples ($P_{i,j}$) within each elementary cell of the voltage domain $\mathcal{D}_v$.

The extrinsic parasitic elements (see Fig. 2), here identified with the automatic linear-regression-based technique in [27], were deembedded from measurements, leading to the intrinsic voltages and currents both versus time (1) and (2) and versus the auxiliary bitemporal domain $(\tau_A,\ \tau_B)$ (3) and (4). With the input power levels adopted, the intrinsic voltage waveforms $\underline{\mathcal{V}}(\tau_A,\ \tau_B)$ were found sweeping the domain $\mathcal{D}_v$, with $v_G \in [-8\,,\ 0]$ V and $v_D \in [0\,,\ 77]$ V. This domain was discretized by choosing $\Delta v_G = 0.8$ mV and $\Delta v_D = 7.7$ mV, corresponding to $N_G = 1000$ and $N_D = 10\,000$ points on the gate and drain axis, respectively. The auxiliary time axes τ_A and τ_B were discretized by assuming $L = K = 2^9$ time instants within the T_A and T_B periods, which led to $\Delta\tau_A = 0.71$ ps and $\Delta\tau_B = 0.97$ ps. With the discretization of voltage and auxiliary bitemporal axes adopted, the numbers $P_{i,j}$ of intrinsic voltage samples $\underline{\mathcal{V}}(\tau_{A,lp}, \tau_{B,kp})$ within each elementary voltage cell $(i,\ j)$ were distributed, as shown in Fig. 4. The number of elementary voltage cells holding two or more samples was found to be about 7800. The resulting linear system of equations obtained by imposing (33) and (34) within each $(i,\ j)$ voltage cell was made of about 70 000 equations to be solved with respect to the $4N_B = 440$ unknown displacement charge spectral components $\underline{Q}^{a}_{n,m}$ and $\underline{Q}^{b}_{n,m}$ (two systems of equations can be separately solved for the gate and drain charges). The Q/V model charge functions $q_G(\underline{v})$ and $q_D(\underline{v})$, obtained by processing the charge waveforms through the NFS operator (26), are shown in Fig. 5 (gate) and Fig. 6 (drain). Contours at constant function values are also plotted in Figs. 5 and 6.

Conduction current spectral components $\underline{F}^{a}_{n,m}$ and $\underline{F}^{b}_{n,m}$ were then obtained by (16) and, with similar application of the NFS operator, the I/V characteristics were also evaluated. The extracted drain current reference characteristic $f_D\left(\underline{v}\right)$ is shown in Fig. 7. For illustrative purposes, $f_D\left(\underline{v}\right)$ is also plotted in

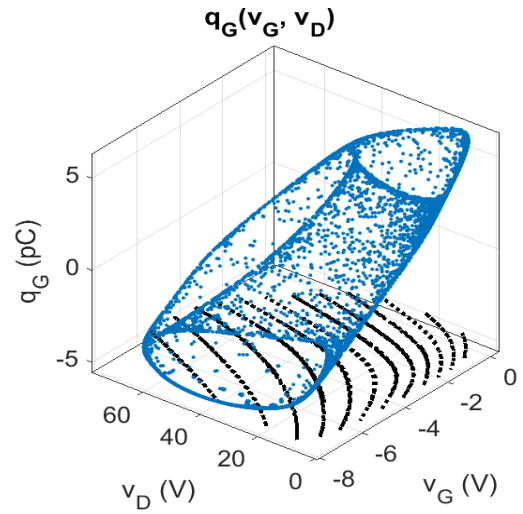

Fig. 5. Gate charge $q_G(v_G, v_D)$ samples as a function of voltage (blue dots). Contours at constant charge values (black dotted lines).

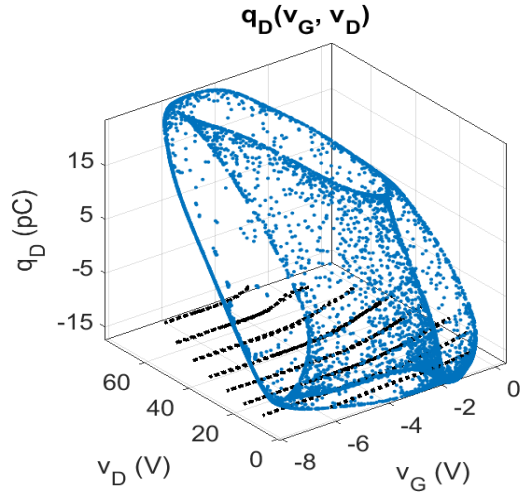

Fig. 6. Drain charge $q_D(v_G, v_D)$ samples as a function of voltage (blue dots). Contours at constant charge values (black dotted lines).

Fig. 8 in the classic format of I/V curves, showing a plausible behavior. Since the forward operation of the gate junction was never involved by the dynamic regime adopted, the gate I/V characteristic $f_G(\underline{v})$ was found to be practically zero over the voltage domain $\mathcal{D}_v$. All the model functions were implemented into linearly interpolated LUTs.

Hereinafter, $f'_D(\underline{v}, \vartheta, x)$ will indicate the generic drain current accounting for any temperature ϑ and charge trapping state x, while the drain conduction current $f_D(\underline{v})$ is that extracted under steady-state conditions with $\vartheta = \hat{\vartheta}$ and $x = \hat{X}$ so that $f_D(\underline{v}) \equiv f'_D(\underline{v}, \hat{\vartheta}, \hat{X})$. Then, $f'_D(\underline{v}, \vartheta, x)$ can be modeled for above cutoff, periodic steady-state operation regime by an equivalent voltage [23] as follows:

$$f'_D(\underline{v}, \vartheta, x) \cong [1 + \alpha_{\vartheta m} \cdot (\vartheta - \hat{\vartheta})] \cdot f'_D(v_{\text{Geq}}, v_D, \hat{\vartheta}, \hat{X}), \tag{35}$$

$$v_{\text{Geq}} = v_G + \alpha_{\vartheta t} \cdot (\vartheta - \hat{\vartheta}) + \alpha_x \cdot (x - \hat{X}). \tag{36}$$

The instantaneous channel temperature ϑ is obtained by $\vartheta = \vartheta_B + R_\vartheta \cdot P_0$, where ϑ_B is the measured baseplate

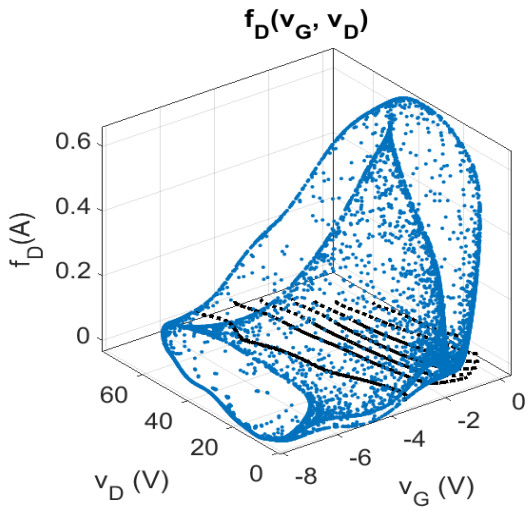

Fig. 7. Drain conduction current $f_D(v_G, v_D)$ samples as a function of voltage (blue dots). Contours at constant charge values (black dotted lines).

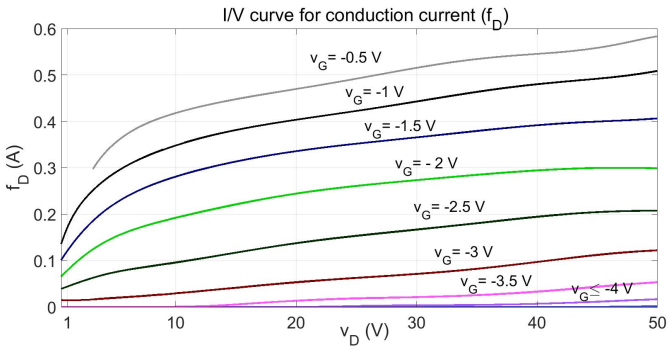

Fig. 8. I/V curve for the conduction current extracted under steady-state conditions: $f_D(\underline{v})$ versus v_D, with v_G as a parameter.

temperature, P_0 is the average dissipated power, and $R_\vartheta \simeq 14$ °C/W as provided by the foundry. The parameters $\alpha_{\vartheta m} = -2$ mA/°C and $\alpha_{\vartheta t} = 1.5$ mV/°C, which account for temperature-dependent carrier mobility and threshold voltage shift, respectively, were obtained from the I/V curves extracted with the proposed method at different baseplate temperatures.

The charge trapping state was here assumed as unambiguously determined by the voltage peaks $\check{v}_G$ (negative) and $\hat{v}_D$ (positive) reached. For an operating regime above the cutoff of the low-frequency trapping effects [8], the trap state deviations were quantified by the following normalized formulation:

$$X_0(\check{v}_G, \hat{v}_D) - \hat{X} = \frac{f'_D(v_G^s, v_D^s, \hat{\vartheta}, X_0(\check{v}_G, \hat{v}_D)) - f'_D(v_G^s, v_D^s, \hat{\vartheta}, \hat{X})}{f'_D(v_G^s, v_D^s, \hat{\vartheta}, \hat{X})} \tag{37}$$

where (v_G^s, v_D^s) represents a current-sensing point on the voltages plane (a point in the saturation region was actually adopted). The current $f'_D(v_G^s, v_D^s, \hat{\vartheta}, X_0(\check{v}_G, \hat{v}_D))$, to be possibly compensated for any temperature discrepancy with respect to the reference case, is the one measured at the charge trapping state X_0 set by the actual voltage peaks $(\check{v}_G, \hat{v}_D)$. By performing various acquisitions under different steady-state regimes (i.e., with different voltage peaks), the trap

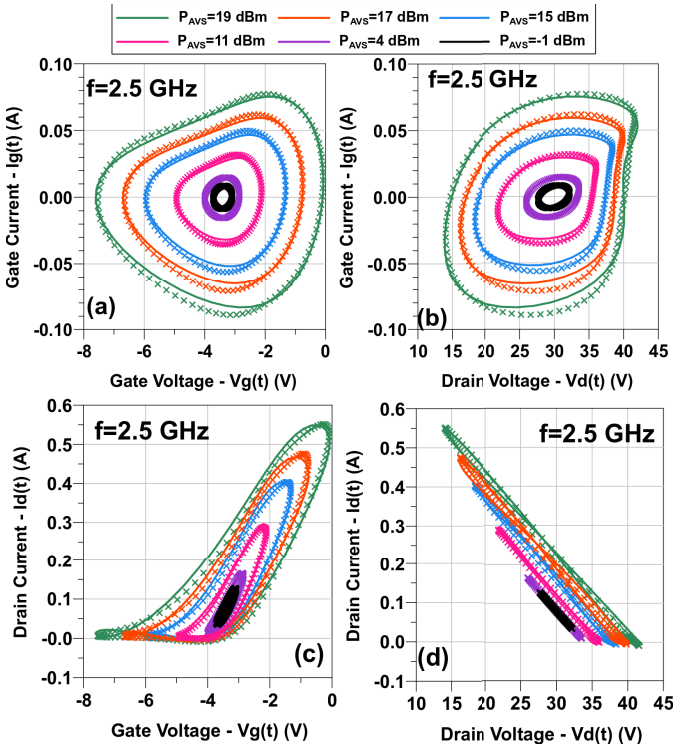

Fig. 9. Measured (x) and modeled (continuous line) GaN HEMT intrinsic current loci. CW excitations at 2.5 GHz: $Z_{L1} = 48.6\ \Omega\angle 177°$, $Z_{L2} = 45.9\ \Omega\angle -179°$, and $Z_{L3} = 49.3\ \Omega\angle -172°$: (a) i_G versus v_G, (b) i_G versus v_D, (c) i_D versus v_G, and (d) i_D versus v_D.

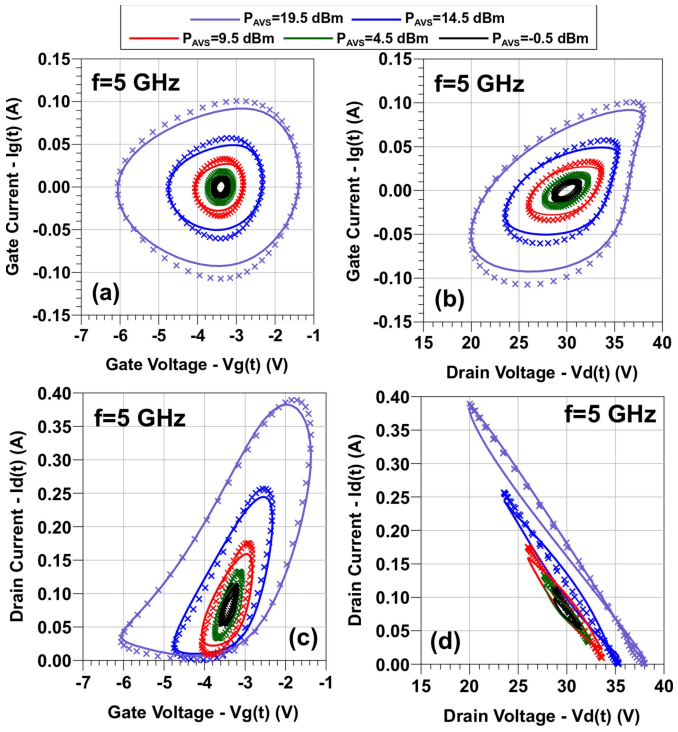

Fig. 10. Measured (x) and modeled (continuous line) GaN HEMT intrinsic current loci. CW excitation at 5 GHz: $Z_{L1} = 45.9\ \Omega\angle -179°$, $Z_{L2} = 54.0\ \Omega\angle 179°$, and $Z_{L3} = 57.6\ \Omega\angle -166°$: (a) i_G versus v_G, (b) i_G versus v_D, (c) i_D versus v_G, and (d) i_D versus v_D.

state deviations (37) were characterized and eventually linearly approximated over the entire voltage domain $\mathcal{D}_v$, obtaining $\alpha_x = -0.8$ V by using (36).

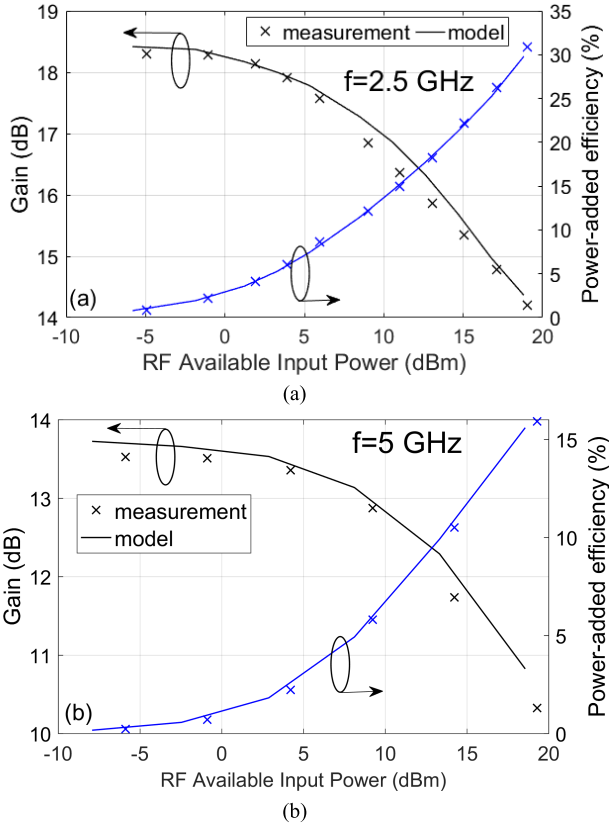

Fig. 11. (a) CW test at 2.5 GHz and (b) 5 GHz. Measurements (x) versus model (continuous line). Load impedance terminations as in Fig. 9 (2.5 GHz) and Fig. 10 (5 GHz).

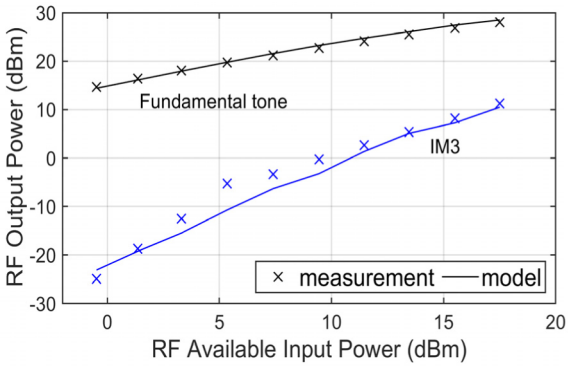

Fig. 12. IMD Test at 2.5 MHz with $\Delta f = 20$ MHz. Measurements (x) versus model (continuous line). Load impedance terminations as in Fig. 9.

The extracted GaN HEMT model has been experimentally validated under CW operation at 2.5 GHz and 5 GHz in a 50-Ω environment. Gate and drain current loci versus voltages are compared to the measurements in Fig. 9 (2.5 GHz) and Fig. 10 (5 GHz) at different available input power levels, whereas gain and power-added efficiency are shown in Fig. 11. An intermodulation distortion validation test has been eventually carried out by applying two tones at the gate DUT input with $f_0 = 2.5$ GHz central frequency and $\Delta f = 20$ MHz tone spacing. The fundamental tone and third-order intermodulation product versus the available input power are shown in Fig. 12. The accurate predictions of measured results validate the proposed modeling approach.

VI. Conclusion

This article proposes a measurement-based method for the global extraction of nonlinear transistor models. A new nonlinear sampling function (NFS) operator, which links waveforms of electrical variables to parent algebraic voltage functions, has been introduced. The operator allows a robust extraction of conduction current I/V characteristics and charge Q/V functions from the current spectra measured under large-signal two-tone two-port quasi-periodic excitation. The procedure is accomplished by solving an overdetermined global system of linear equations with respect to the unknown spectral components of the charge waveforms. The proposed method is especially suitable for automatic model generation.

Acknowledgment

The authors wish to thank Prof. D. M. M.-P. Schreurs from ESAT-TELEMIC, KU Leuven, Leuven, Belgium, for the access to equipment and V. Di Giacomo Brunel, D. Floriot, and C. Chang from United Monolithic Semiconductors, Villebon-sur-Yvette, France, for providing the GaN devices.

References

[1] S. M. Homayouni, D. M. M.-P. Schreurs, G. Crupi, and B. K. J. C. Nauwelaers, "Technology-independent Non-Quasi-Static table-based nonlinear model generation," *IEEE Trans. Microw. Theory Techn.*, vol. 57, no. 12, pp. 2845–2852, Dec. 2009.

[2] G. P. Gibiino, A. Santarelli, and F. Filicori, "Charge-conservative GaN HEMT nonlinear modeling from non-isodynamic multi-bias S-parameter measurements," *Int. J. Microw. Wireless technol.*, vol. 11, nos. 5–6, pp. 431–440, Feb. 2019.

[3] D. E. Root, "Analysis and exact solutions of relaxation-time differential equations describing non quasi-static large signal FET models," in *Proc. 24th Eur. Microw. Conf.*, Oct. 1994, pp. 854–859.

[4] D. Siriex, O. Noblanc, D. Barataud, E. Chartier, C. Brylinski, and R. Quere, "A CAD-oriented nonlinear model of SiC MESFET based on pulsed I(V), pulsed S-parameter measurements," *IEEE Trans. Electron Devices*, vol. 46, no. 3, pp. 580–584, Mar. 1999.

[5] A. Santarelli *et al.*, "A double-pulse technique for the dynamic I/V characterization of GaN FETs," *IEEE Microw. Wireless Compon. Lett.*, vol. 24, no. 2, pp. 132–134, Feb. 2014.

[6] A. M. Angelotti, G. P. Gibiino, C. Florian, and A. Santarelli, "Narrow-pulse-width double-pulsed S-parameters measurements of 100-nm GaN-on-Si HEMTs," in *Proc. 14th Eur. Microw. Integr. Circuits Conf. (EuMIC)*, Paris, France, Sep. 2019, pp. 17–20.

[7] C. F. Goncalves, L. C. Nunes, P. M. Cabral, and J. C. Pedro, "Conservative current and charge data extracted from pulsed S-parameter measurements for GaN HEMT PA design," in *IEEE MTT-S Int. Microw. Symp. Dig.*, Jun. 2017, pp. 1065–1068.

[8] G. P. Gibiino, A. Santarelli, and F. Filicori, "A GaN HEMT global large-signal model including charge trapping for multibias operation," *IEEE Trans. Microw. Theory Techn.*, pp. 1–14, Nov. 2018.

[9] G. P. Gibiino, C. Florian, A. Santarelli, T. Cappello, and Z. Popović, "Isotrap pulsed IV characterization of GaN HEMTs for PA design," *IEEE Microw. Wireless Compon. Lett.*, vol. 28, no. 8, pp. 672–674, Aug. 2018.

[10] G. Avolio *et al.*, "Millimeter-wave FET nonlinear modelling based on the dynamic-bias measurement technique," *IEEE Trans. Microw. Theory Techn.*, vol. 62, no. 11, pp. 2526–2537, Nov. 2014.

[11] J. Xu, R. Jones, S. A. Harris, T. Nielsen, and D. E. Root, "Dynamic FET model–DynaFET–for GaN transistors from NVNA active source injection measurements," in *IEEE MTT-S Int. Microw. Symp. Dig.*, Jun. 2014, pp. 1–3.

[12] T. M. Martín-Guerrero, J. D. Baños-Polglase, and C. Camacho-Peñalosa, "Frequency domain-based extraction method of quasi-static nonlinear state functions from large-signal microwave measurements," *Int. J. Microw. Opt. Technol.*, vol. 1, no. 1, pp. 90–99, Jun. 2006.

[13] T. M. Martin-Guerrero, J. D. Banos-Polglase, C. Camacho-Penalosa, M. Fernandez-Barciela, D. G. Morgan, and P. J. Tasker, "Frequency domain-based approach for nonlinear quasi-static FET model extraction from large-signal waveform measurements," in *Proc. Eur. Microw. Integr. Circuits Conf.*, Sep. 2006, pp. 441–444.

[14] S. Perez-Parras, T. M. Martin-Guerrero, J. D. Banos-Polglase, and C. Camacho-Penalosa, "Frequency domain-based method for a two-port nonlinear quasi-static model extraction from large-signal waveforms," in *Proc. 13th Eur. Microw. Integr. Circuits Conf. (EuMIC)*, Sep. 2018, pp. 69–72.

[15] D. Schreurs, J. Verspecht, B. Nauwelaers, A. Van de Capelle, and M. Van Rossum, "Direct extraction of the non-linear model for two-port devices from vectorial non-linear network analyzer measurements," in *Proc. 27th Eur. Microw. Conf.,*, Oct. 1997, pp. 921–926.

[16] D. M. M.-P. Schreurs, J. Verspecht, S. Vandenberghe, and E. Vandamme, "Straightforward and accurate nonlinear device model parameter-estimation method based on vectorial large-signal measurements," *IEEE Trans. Microw. Theory Techn.*, vol. 50, no. 10, pp. 2315–2319, Oct. 2002.

[17] D. G. Morgan, G. D. Edwards, A. Phillips, and P. J. Tasker, "Full extraction of PHEMT state functions using time domain measurements," in *IEEE MTT-S Int. Microw. Symp. Dig.*, vol. 2, May 2001, pp. 823–826.

[18] F. Verbeyst and M. V. Bossche, "Real-time and optimal PA characterization speeds up PA design," in *Proc. 34th Eur. Microw. Conf.*, Oct. 2004, pp. 431–434.

[19] P. Roblin, S. J. Doo, X. Cui, G. H. Jessen, D. Chaillot, and J. Strahler, "New ultra-fast real-time active load-pull measurements for high speed RF power amplifier design," in *IEEE MTT-S Int. Microw. Symp. Dig.*, Jun. 2007, pp. 1493–1496.

[20] M. C. Currás-Francos, P. J. Tasker, M. Fernández-Barciela, S. S. O'Keefe, Y. Campos-Roca, and E. Sánchez, "Direct extraction of nonlinear FET I-V functions from time domain large signal measurements," *Electron. Lett.*, vol. 34, no. 21, pp. 1993–1994, Oct. 1998.

[21] M. C. Currás-Francos, P. J. Tasker, M. Fernández-Barciela, Y. Campos-Roca, and E. Sánchez, "Direct extraction of nonlinear FET Q-V functions from time domain large signal measurements," *IEEE Microw. Guided Wave Lett.*, vol. 10, no. 12, pp. 531–533, Dec. 2000.

[22] Y. Ko *et al.*, "Artificial neural network model of SOS-MOSFETs based on dynamic large-signal measurements," *IEEE Trans. Microw. Theory Techn.*, vol. 62, no. 3, pp. 491–501, Mar. 2014.

[23] D. Niessen, G. P. Gibiino, R. Cignani, A. Santarelli, D. M. M.-P. Schreurs, and F. Filicori, "Charge-controlled GaN FET modeling by displacement current integration from frequency-domain NVNA measurements," *IEEE Trans. Microw. Theory Techn.*, vol. 64, no. 12, pp. 4382–4393, Dec. 2016.

[24] F. Filicori and V. A. Monaco, "Computer-aided design of non-linear microwave circuits," *Alta Frequenza*, vol. 57, no. 7, pp. 355–378, 1988.

[25] I. Angelov *et al.*, "On the large-signal modeling of high power AlGaN/GaN HEMTs," in *IEEE MTT-S Int. Microw. Symp. Dig.*, Jun. 2012, pp. 1–3.

[26] J. C. Pedro, D. E. Root, J. Xu, and L. C. Nunes, *Nonlinear Circuit Simulation and Modeling: Fundamentals for Microwave Design*. Cambridge, U.K.: Cambridge Univ. Press, 2018.

[27] G. P. Gibiino, A. Santarelli, R. Cignani, P. A. Traverso, and F. Filicori, "Measurement-based automatic extraction of FET parasitic network by linear regression," *IEEE Microw. Wireless Compon. Lett.*, vol. 29, no. 9, pp. 598–600, Sep. 2019.

Teresa M. Martín-Guerrero (Member, IEEE) was born in Málaga, Spain. She received the M.Sc. degree in physics from the Universidad de Granada, Granada, Spain, in 1990, and the Ph.D. degree in telecommunication engineering from the Universidad de Málaga, Málaga, in 1995.

In 1991, she joined the Departamento de Ingenieria de Comunicaciones, Universidad de Málaga, where she became a Full Professor in 2016. From 2008 to 2012, she was the Vice-Director for Research with the E. T. S Ingeniería de Telecomunicación, Universidad de Málaga. Her current research interests include microwave and millimeter-wave device characterization and modeling and the analysis, and design of RF nonlinear circuits.

Prof. Martín-Guerrero has been the Chair of the 13th European Microwave Integrated Circuits Conference (EuMIC), Madrid, in September 2018.

Alberto Santarelli (Member, IEEE) received the Laurea degree (cum laude) in electronic engineering and the Ph.D. degree in electronics and computer science from the University of Bologna, Bologna, Italy, in 1991and 1996, respectively.

From 1996 to 2001, he was a Research Assistant with the Research Center for Computer Science and Communication Systems, Italian National Research Council, Bologna. In 2001, he joined the Department of Electrical, Electronic and Information Engineering "Guglielmo Marconi"-DEI, University of Bologna, where he is currently an Associate Professor. During his academic career, he has been a Lecturer of applied electronics, high-frequency electronics, and power electronics. His current research interests include the nonlinear characterization and modeling of electron devices and the nonlinear microwave circuit design.

Gian Piero Gibiino (Member, IEEE) received the dual Ph.D. degree from the University of Bologna, Bologna, Italy, and KU Leuven, Leuven, Belgium, in 2016.

Since 2012, he has been with the Department of Electrical Engineering "Guglielmo Marconi"-DEI, University of Bologna, where he is currently a Post-Doctoral Research Fellow. His research interests include RF electron devices and power amplifiers nonlinear modeling, electronic instrumentation, and microwave measurements.

Dr. Gibiino is a member of the Italian Association of Electrical and Electronic Measurements (GMEE).

Pier Andrea Traverso (Member, IEEE) was born in Modena, Italy, in 1969. He received the M.S. degree (Hons.) in electronic engineering and the Ph.D. degree in electronic and computer science engineering from the University of Bologna, Bologna, Italy, in 1996 and 2000, respectively.

Since 2002, he has been with the Department of Electrical, Electronic and Information Engineering "Guglielmo Marconi"-DEI, University of Bologna, where he is currently an Associate Professor of Electronic Measurement. From 2000 to 2002, he was awarded a research grant by the Italian National Research Council (CSITE-CNR Institute, Bologna) for research activity concerning microwave electron device characterization and nonlinear empirical modeling. His main research interests are in the areas of nonlinear dynamic system characterization and empirical modeling, microwave and millimeter-wave semiconductor device characterization and modeling, smart sensor nodes, and advanced sampling instrumentation and techniques. He is the coauthor of more than 100 international journal/conference technical papers.

Dr. Traverso is a member of the Italian Association of Electrical and Electronic Measurement (GMEE).

Carlos Camacho-Peñalosa (Life Senior Member, IEEE) received the Ingeniero de Telecomunicación and Dr.Ing. degrees from the Universidad Politécnica de Madrid, Madrid, Spain, in 1976 and 1982, respectively.

From 1976 to 1989, he was with the Escuela Técnica Superior de Ingenieros de Telecomunicación, Universidad Politécnica de Madrid, as a Research Assistant, an Assistant Professor, and an Associate Professor. From September 1984 to July 1985, he was a Visiting Researcher with the Department of Electronics, Chelsea College, University of London, London, U.K. In 1989, he became a Full Professor at the Universidad de Málaga, Málaga, Spain. He was the Director of the Escuela Técnica Superior de Ingeniería de Telecomunicación from 1991 to 1993, a Vice-Rector 1993 to 1994, and a Deputy Rector in 1994 of the Universidad de Málaga. From 1996 to 2004, he was the Director of the Departamento de Ingeniería de Comunicaciones, Universidad de Málaga. From 2000 to 2003, he was the Co-Head of the Nokia Mobile Communications Competence Centre, Málaga. His research interests include microwave and solid-state circuits, nonlinear systems, and applied electromagnetism. He has been responsible for several research projects on nonlinear microwave circuit analysis, microwave semiconductor device modeling, and applied electromagnetics.

Fabio Filicori received the M.S. degree in electronic engineering from the University of Bologna, Bologna, Italy, in 1974.

In 1974, he joined the Department of Electronics, Computer Science and Systems, University of Bologna, as a Research Assistant and then became an Associate Professor of applied electronics. In 1990, he was a Full Professor of applied electronics with the University of Perugia, Perugia, Italy. In 1991, he joined the Faculty of Engineering, University of Ferrara, Ferrara, Italy, as a Full Professor, where he was responsible for the degree course in electronic engineering. In 1993, he joined the Faculty of Engineering, University of Bologna, as a Full Professor, where he is currently an Adjunct Professor involved in teaching and research activities after retiring in 2016. During his academic career, he has held courses on computer-aided circuit design, electron devices and circuits, and power electronics. His current research interests include computer-aided design techniques for nonlinear microwave circuits, electron device nonlinear modeling, sampling digital instrumentation, and power electronics.

Mr. Filicori has been a member of the Space Technology Committee of the Italian Space Agency and national responsible of several research projects on electronics for the Italian National Research Council. He was the Technical Program Committee Chairman of the European Microwave Integrated Circuit Conference, Rome, Italy, in 2009.